

Influence of PVP template on the formation of porous TiO₂ nanofibers by electrospinning technique for dye-sensitized solar cell

Vijayakumar Elayappan¹ · Pratheep Panneerselvam¹ · Sivasankar Nemala² ·
Karthick S. Nallathambi³ · Subramania Angaiah¹

Received: 12 December 2014 / Accepted: 22 June 2015 / Published online: 10 July 2015
© Springer-Verlag Berlin Heidelberg 2015

Abstract The porous TiO₂ nanofibers were prepared by electrospinning technique using polyvinylpyrrolidone (PVP) as template as well as pore-forming agent at the calcination temperature of 475 °C for 5 h. The influence of various concentrations of PVP (5, 8 and 10 wt%) on the surface area and porosity of the prepared TiO₂ nanofibers (NFs) were studied by using BET-specific surface area analyzer. The TiO₂ NFs obtained by using 5 wt% of PVP had higher surface area and porosity than those obtained by using 8 and 10 wt% of PVP. The prepared electrospun TiO₂ NFs were characterized by using TG analysis, X-ray diffraction, FTIR, FE-SEM and TEM studies. Finally, dye-sensitized solar cells were assembled using the prepared TiO₂ NFs as the photoanode, Pt as the cathode and 0.5 M 1-butyl-3-methylimidazolium iodide, 0.5 M LiI, 0.05 M I₂, 0.5 M 4-tertbutylpyridine in acetonitrile as an electrolyte. Among the three photoanodes, the cell assembled using porous TiO₂ NFs obtained by using 5 wt% of PVP showed higher power conversion efficiency (PCE) of 4.81 % than those obtained by using 8 and 10 wt% of PVP, which showed the lower PCE of 4.13 and 3.42 %, respectively.

1 Introduction

Dye-sensitized solar cells (DSSCs) are low cost, easy fabrication, high efficiency and good alternative solution for converting sunlight to electricity than the silicon-based solar cells. The most efficient DSSCs based on ruthenium complex have energy conversion efficiency of over 12 %. In a typical DSSC operation, the electrons from photoexcited dye molecules are first injected into mesoporous metal oxide and then travel to the current collector and subsequently reach the counter electrode through an external circuit. The dye molecule regains electrons from a redox couple (e.g., I⁻/I₃⁻) in an electrolyte [1, 2]. Recently, one-dimensional (1D) nanostructured metal oxides have attracted much attention because of their unique properties and potential applications in electronics, photonics and other related areas [3, 4]. There are several methods such as hydrothermal, template growth, thermal evaporation, solvothermal and electrospinning to develop one-dimensional nanomaterial's [5–13]. Among these, electrospinning is a very good method to develop nanofibres, and we can generate NFs of different morphologies.

Efficient light-to-energy conversion of DSSCs requires the sensitized electrode with high surface area and high porosity to enhance the light-harvesting capability of the dye adsorbed on the TiO₂ film. TiO₂ is a wide energy band gap (~3.2 eV) photoactive semiconductor material that can absorb UV light. In addition, TiO₂ possesses other desirable features, such as strong oxidizing power, non-toxicity, chemical and biological stability, photoinduced hydrophobicity, high photoactivity, photodurability as well as low cost and good corrosion resistance in aqueous solution. Thus, TiO₂ is a suitable candidate for various applications such as DSSCs, sensors, photoluminescence and photocatalytic [14–

✉ Subramania Angaiah
a.subramania@gmail.com

¹ Electrochemical Energy Research Lab, Centre for Nanoscience and Technology, Pondicherry University, Puducherry 605 014, India

² Department of Metallurgical Engineering and Materials Science, Indian Institute of Technology-Bombay, Mumbai 400076, India

³ School of Electrical and Computer Engineering, Pusan National University, Jangjeon, Geumjeong, Busan 609 735, Republic of Korea

18]. In recent years, one-dimensional nanostructures have attracted significant attention for applications in DSSCs due to their unique structures, low resistance to mass transport, large surface to volume ratios, enhanced charge collection efficiency in terms of speeding up electron transport and slowing recombination as compared to the nanoparticle films [19, 20]. It is also reported that the porous TiO₂ NFs with 3D structures have strong potential for applications in solar cell electrodes because the porous TiO₂ NFs have surface area approximately one to two orders of magnitude larger than continuous fibers [21, 22]. Recently, many reports are available in the literature for the preparation of TiO₂ NFs by electrospinning techniques. But the influence of PVP template on the formation of TiO₂ nanofibres has not been focused [2, 23–25].

Hence, in the present investigation, the influence of PVP template on the formation of TiO₂ NFs by electrospinning technique is studied in detail. The surface morphology, porosity and pore volume of calcined TiO₂ nanofibres are also studied. The prepared TiO₂ NFs obtained by using different wt% of PVP are used as photoanodes for dye-sensitized solar cell, and their photovoltaic performances are studied under a simulated solar irradiation for comparison.

2 Experimental

2.1 Materials

Fluorine-doped tin oxide glass (FTO, TEC-7 and 2.2 mm thick) was used as the substrate for DSSC device. Titanium (IV) isopropoxide (99 %), polyvinylpyrrolidone (PVP) and di-tetrabutyl ammonium cis-bis(isothiocyanato) bis (2, 2'-bipyridyl-4, 4'-dicarboxylato) ruthenium (II) (N719 dye) were procured from Sigma-Aldrich. Ethanol and acetic acid were procured from Merck India Ltd. All these chemicals are analytical grade and used as received without any further purification.

2.2 Preparation of TiO₂ NFs

In a typical procedure, 0.01 M titanium isopropoxide was mixed with 0.04 M acetic acid and stirred for 10 min. This solution was mixed separately with different wt% of PVP (5, 8 and 10 wt%) solution and then stirred for 6 h in a closed bottle to get Ti(OH)₄-PVP composite viscous solutions [16, 18]. The yellowish Ti(OH)₄-PVP composite viscous solutions were loaded in 10-ml syringe equipped with 27-G stainless steel needle. The electrospinning was carried out at a high voltage of 15.3 kV in a flow rate of 1 mL/h. The distance between the needle tip and the collector was 12 cm, and the humidity of the chamber was

maintained at <35 % to get electrospun TiO₂ nanofibrous precursor mats over drum collector. They were collected and vacuum dried at 60 °C for 12 h and then calcined in a muffle furnace (Technico, India) at 475 °C for 5 h at the heating rate of 5 °C min⁻¹ in air atmosphere to get pure TiO₂ NFs.

2.3 Characterization of TiO₂ NFs

The phase formation and/or complete decomposition temperature of the electrospun TiO₂ fibrous precursor was understood by thermogravimetric (TG) analysis (TA Instruments, Model: Q600 SDT). The structural characterization of the prepared TiO₂ NFs was studied by using X-ray diffraction technique (Rigaku, Ultima IV) with nickel-filtered Cu-K α radiation in a range from 20° to 80° with an increment of 0.05°. The Fourier transform infrared (FTIR) spectral studies were carried out in the wavenumber range of 4000–400 cm⁻¹ (Thermo Nicolet, Model: 6700). The surface morphology was examined by using scanning electron microscope (Hitachi, Model: s-4200). Surface area, pore size and pore volume of the prepared TiO₂ NFs were analyzed by using Brunauer–Emmett–Teller (BET) nitrogen adsorption method (Micromeritics, Model: Gemini 2390-t). Electrochemical AC impedance measurements (Biologic-VSP, France) were taken at room temperature in the frequency range of 1 mHz–100 kHz with the AC amplitude of 10 mV under AM 1.5 sun illumination with a light intensity of 100 mW cm⁻² to determine the charge transfer resistance between the conducting oxide (FTO) and TiO₂ NFs obtained by using 5, 8 and 10 wt% of PVP and the interface between TiO₂ NFs/dye/electrolyte.

2.4 Preparation of TiO₂ NFs paste

The different photoanode pastes were prepared by mixing an optimized amount of 30 wt% of prepared TiO₂ NFs (obtained by using different wt% of PVP) along with 15 wt% of ethyl cellulose, 50 wt% of terpineol and 5 wt% of dibutyl phthalate. They were then stirred well followed by a slow evaporation to get TiO₂ pastes. The pastes were coated with a thickness of 10–12 μ m on each FTO glass plate by the doctor blade technique and sintered at 450 °C for 30 min [26].

2.5 Fabrication of DSSCs

The FTO glass plates were cleaned with a detergent solution in an ultrasonic water bath for 30 min followed by cleaning in deionized water, acetone and ethanol for 10 min each and then dried in an open air at 30 °C. Scotch tape was employed as a spacer to control the film thickness and to provide non-coated areas for electrical

contact. The paste was prepared by using TiO₂ NFs obtained by using different wt% of PVP and coated on pretreated FTO glass substrates by the doctor blade technique. They were then dried at 30 °C for 10 min, followed by annealing at 450 °C in a muffle furnace at 5 °C min⁻¹ for 30 min to remove the organic ingredients and to facilitate the interconnection among the TiO₂ NFs. The thickness of the films was found to be around 10–12 μm. The area of the photoanodes was 0.20 cm². After cooling to 80 °C, the TiO₂ electrodes were immersed into the purified 0.3 mM N719 dye solution [di-tetrabutyl ammonium cis-bis(isothiocyanato) bis (2,2'-bipyridyl-4,4'-dicarboxylato) ruthenium(II)] for 12 h at room temperature [27]. After completion of the dye adsorption, the films were rinsed with pure ethanol to remove the excess dye. In the counter electrode, a pair of hole was drilled to inject the electrolyte later and subsequently cleaned in an ultrasonic bath with ethanol and acetone (1:1 volume ratio) for 5 min. Then, the standard Pt paste (Dyesol Ltd) was applied using the doctor blade technique, followed by sintering in a muffle furnace at 450 °C for 30 min. DSSCs were assembled using dye-sensitized TiO₂ NFs as photoanodes and Pt-coated FTO glass plate as counter electrode for each cell. The dye-adsorbed TiO₂ NFs-based electrodes (working electrode) were sealed with the counter electrode using thermal adhesive film (Surlyn, DuPont 1702, 60 μm thick) by a hot press to avoid the short circuiting of the cells. A drop of the prepared electrolyte solution of 0.5 M 1-butyl-3-methylimidazolium iodide, 0.5 M LiI, 0.05 M I₂, 0.5 M 4-tertbutylpyridine in acetonitrile was introduced inside the cell through the hole drilled in the counter electrode [28]. The holes were then sealed with Surlyn strip. The resulting active areas of the cells were found to be 0.20 cm².

2.6 Photovoltaic performance of DSSCs

Photovoltaic cell is a device, which converts incident light to electrical energy. Generation of electrical power under illumination is achieved by the capability of the photovoltaic device to produce voltage over an external load and current through the load at the same time. The performance of DSSCs was determined by a calibrated AM 1.5 solar illumination (Newport, Oriel instruments, USA, 150 W, Model: 67005) with a light intensity of 100 mW cm⁻² calibrated using standard monocrystalline silicon solar cell (Newport, Oriel instruments, Model: 91150 V) and a computer-controlled digital source meter (Keithley, Model: 2420). The photoelectrochemical parameters, i.e., the fill factor (FF) and light-to-electricity conversion efficiency (η), were calculated using the following equations:

$$\eta (\%) = \frac{V_{\max} J_{\max}}{P_{\text{in}}} \times 100 = \frac{V_{\text{oc}} J_{\text{sc}} FF}{P_{\text{in}}} \times 100$$

$$FF = \frac{V_{\max} J_{\max}}{V_{\text{oc}} J_{\text{sc}}}$$

where J_{sc} is the short-circuit current density (mA cm⁻²), V_{oc} is the open-circuit voltage (V), P_{in} is the incident light power (mW cm⁻²), and J_{\max} and V_{\max} are the current density (mA cm⁻²) and voltage (V) in the J - V curves, respectively, at the point of maximum power output. All the fabrication steps and characterization measurements were carried out in an ambient environment without a protective atmosphere.

3 Results and discussion

3.1 TG analysis

Figure 1 shows the TG curves of electrospun TiO₂ fibrous precursor mats obtained using different wt% of PVP. The analysis is performed at the heating rate of 10 °C min⁻¹ in air atmosphere up to 700 °C. As the temperature increases from 30 to 100 °C, a small weight loss of 10–15 % is observed in all the three TiO₂ fibrous mats due to loss of moisture in the precursor mats. For the temperature between 100 and 350 °C, a gradual weight loss of 10–14 % is observed due to the degradation of PVP on the side chain as well as decomposition of low molecular weight organic matter. The decomposition of main chain of PVP continues from 350 to 475 °C, and the corresponding weight loss is found to be 22–34 % for all the three TiO₂ fibrous precursor samples. Subsequently, a steep slope indicates the huge weight loss of PVP due to complete decomposition up

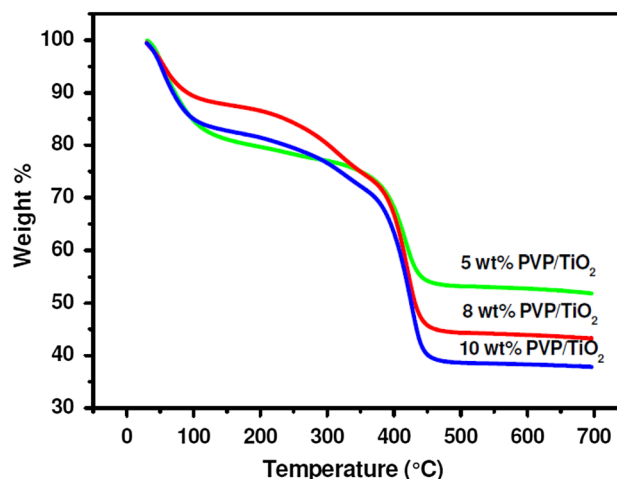


Fig. 1 TG curves of electrospun TiO₂ fibrous precursor mats

to 475 °C. The pure anatase TiO₂ nanofiber remains at temperature greater than 475 °C.

3.2 XRD studies

Figure 2 shows the XRD pattern of TiO₂ NFs obtained by using different wt% of PVP, calcined at 475 °C for 5 h. The NFs calcined at this temperature present several characteristic diffraction peaks, and their corresponding miller indices (*hkl*) of 2θ values clearly index the anatase phase of TiO₂ (JCPDS 21-1272). The highest intensity diffraction peak of 25.26° for the (101) crystal plane is the representative of anatase phase of TiO₂. The absence of diffraction peaks at 27° and 31° reveals that the sample is free from the rutile structure of TiO₂. In general, the presence of a diffraction peak at 30° indicates the presence of crystal imperfection or the absence of long-range ordering in the TiO₂ NFs. This suggests that phase pure anatase TiO₂ with a tetragonal anatase structure is formed at 475 °C [2, 16].

3.3 FTIR studies

Figure 3a, b shows the Fourier transform infrared (FTIR) spectra of electrospun TiO₂ fibrous precursor mat before and after calcination at 475 °C for 5 h. In Fig. 3a, the absorption bands in the range of 1000–1800 cm⁻¹ correspond to the bending and stretching frequencies of PVP. The peak at 650 cm⁻¹ corresponds to the Ti–O bond, which confirms the formation of TiO₂ within PVP/TiO₂ composite NFs. The characteristic peaks of PVP are identified at 1665 cm⁻¹ (stretching mode of C=O) and 1288 cm⁻¹ (stretching mode of C–N). The broad peak

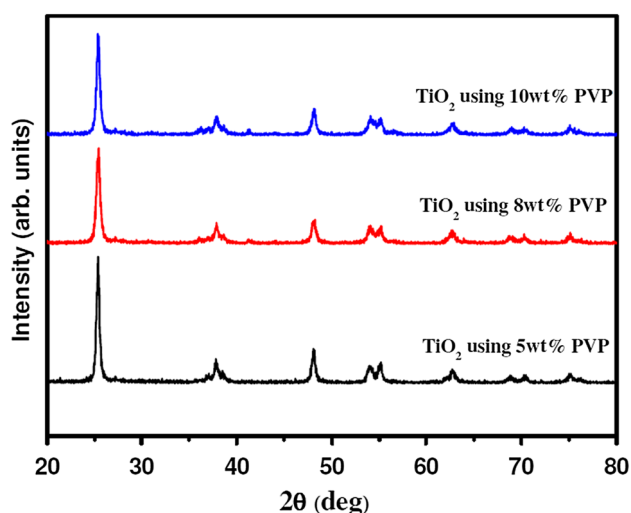


Fig. 2 XRD patterns of TiO₂ NFs obtained by using different wt% of PVP at 475 °C for 5 h

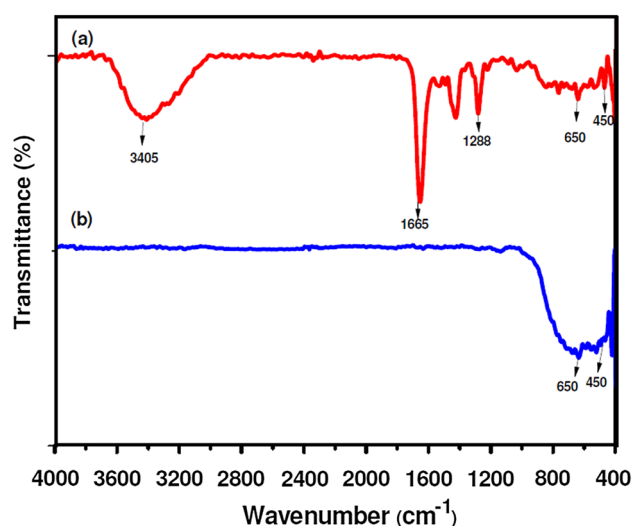


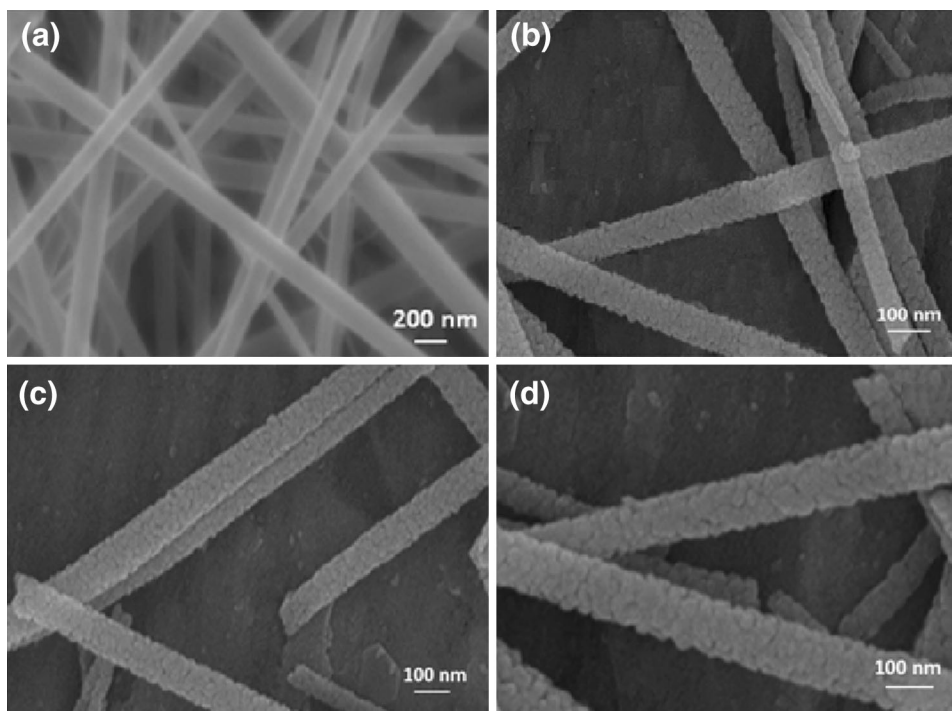
Fig. 3 FTIR spectrum of **a** electrospun TiO₂ fibrous precursor mat and **b** TiO₂ NFs obtained at 475 °C for 5 h

centered at 3405 cm⁻¹ in the spectrum is attributed to the O–H stretching mode of physically adsorbed water molecule. In Fig. 3b, the peaks corresponding to PVP and physically adsorbed water completely disappeared after calcination at 475 °C, suggesting the complete removal of the organic components. Moreover, the shift from 650 cm⁻¹ corresponds to the characteristic peak of Ti–O stretching mode. The peak at 450 cm⁻¹ demonstrates the rearrangement in the crystal structure of TiO₂ during calcination at 475 °C [29, 30].

3.4 Morphological studies

Figure 4a–d shows the FE-SEM images of electrospun TiO₂ NFs before and after calcination at 475 °C for 5 h. From Fig. 4a, the average diameters of the electrospun TiO₂ fibrous mats obtained by using different weight percentages of PVP (5, 8 and 10 wt%) are found to be 200–250 nm. Figure 4b–d depicts that after calcination their average diameters are found to be 98, 121 and 127 nm, respectively. This clearly indicates that the increasing PVP content increases the fiber diameter and hence decreases the overall surface to volume ratio. This is due to the low polymer concentration, which has more solvent to evaporate and takes longer time to solidify. This generates nanofibers with thinner diameter [20]. It reveals that the decreasing the concentration to 5 wt% results in less fiber diameter (98 nm) leading to larger surface to volume ratio. Further, decreasing the concentrations of PVP reduces the viscosity, and hence, the formation of TiO₂ NFs is difficult. Figure 5a–c illustrates the TEM images with different magnifications of TiO₂ NFs obtained by using 5 wt% PVP. It shows the TEM images of a single

Fig. 4 **a** SEM image of electrospun TiO₂ fibrous mat obtained by using 5 wt% of PVP before calcination, **b–d** FE-SEM image of TiO₂ NFs obtained by using 5, 8 and 10 wt% of PVP after calcination at 475 °C



nanofibers consisting of numerous TiO₂ nanocrystallites. Figure 5d shows that the SAED pattern of TiO₂ NFs obtained by using 5 wt% of PVP confirms the formation of polycrystalline anatase phase that has good agreement with the XRD result.

3.5 BET surface analysis

The surface area, pore size and pore volume of TiO₂ obtained using different wt% of PVP containing TiO₂ fibrous mat are calculated from isotherm data obtained by BET method providing adsorption and desorption in the relative pressure (p/p_0) range of 0.05–0.99. The Barrett–Joyner–Halenda method determines the nitrogen adsorption and desorption volume. Table 1 presents the BET surface area, pore volume and pore size of TiO₂ NFs obtained from different wt% of PVP. Among them, TiO₂ NFs obtained by using 5 wt% of PVP show higher surface area, pore volume and pore size than those obtained by using 8 and 10 wt% of PVP. It is because the size of TiO₂ NFs obtained by using 5 wt% PVP is thinner than the fibers obtained by using 8 and 10 wt% of PVP. It reveals that the surface area of TiO₂ NFs can be controlled by the amount of PVP used.

3.6 Photovoltaic performance of DSSCs

Figure 6 shows the photocurrent density–voltage (J – V) curves for DSSCs assembled using TiO₂ NFs obtained

by using different wt% of PVP at a light intensity of 100 mW cm⁻² under the standard global AM 1.5 irradiation. Table 2 summarizes their photovoltaic parameters. It shows that the porous TiO₂ NFs obtained by using 5 wt% of PVP exhibit the higher efficiency of 4.81 % than those obtained by using 8 and 10 wt% of PVP. This may be due to the highly porous nature of TiO₂ NFs with larger surface to volume ratio that are attributed to the higher amount of dye adsorption on the porous TiO₂ NFs surface [31]. It increases the light-harvesting effect, which increases the PCE of the DSSC.

3.7 Electrochemical impedance studies

The electrochemical impedance measurements are taken to study the interfacial characteristics of TiO₂ NFs photoanode by determining their charge transfer resistance. Figure 7 shows the Nyquist plots of the DSSCs based on TiO₂ NFs using different wt% of PVP. The obtained Nyquist plots consist of two semicircles: the first semicircle denotes redox reaction of I^-/I_3^- at the Pt/electrolyte interface (R_{ct1}) and the second largest semicircle denotes electron transfer at the TiO₂ NFs/dye/electrolyte interface (R_{ct2}). It also shows that the recombination suppressed with decrease in the wt% of PVP-based TiO₂ NFs from 10 to 5 wt%. The overall charge transfer resistance value for TiO₂ NFs obtained by using 5 wt% of PVP is lesser when compared to 8 and 10 wt% of PVP. It reveals that the TiO₂ NFs/dye/electrolyte interface is effectively accelerated the

Fig. 5 TEM images of the TiO₂ NFs obtained by using 5 wt% PVP; **a–c** High-resolution image at different magnifications and **d** SAED pattern

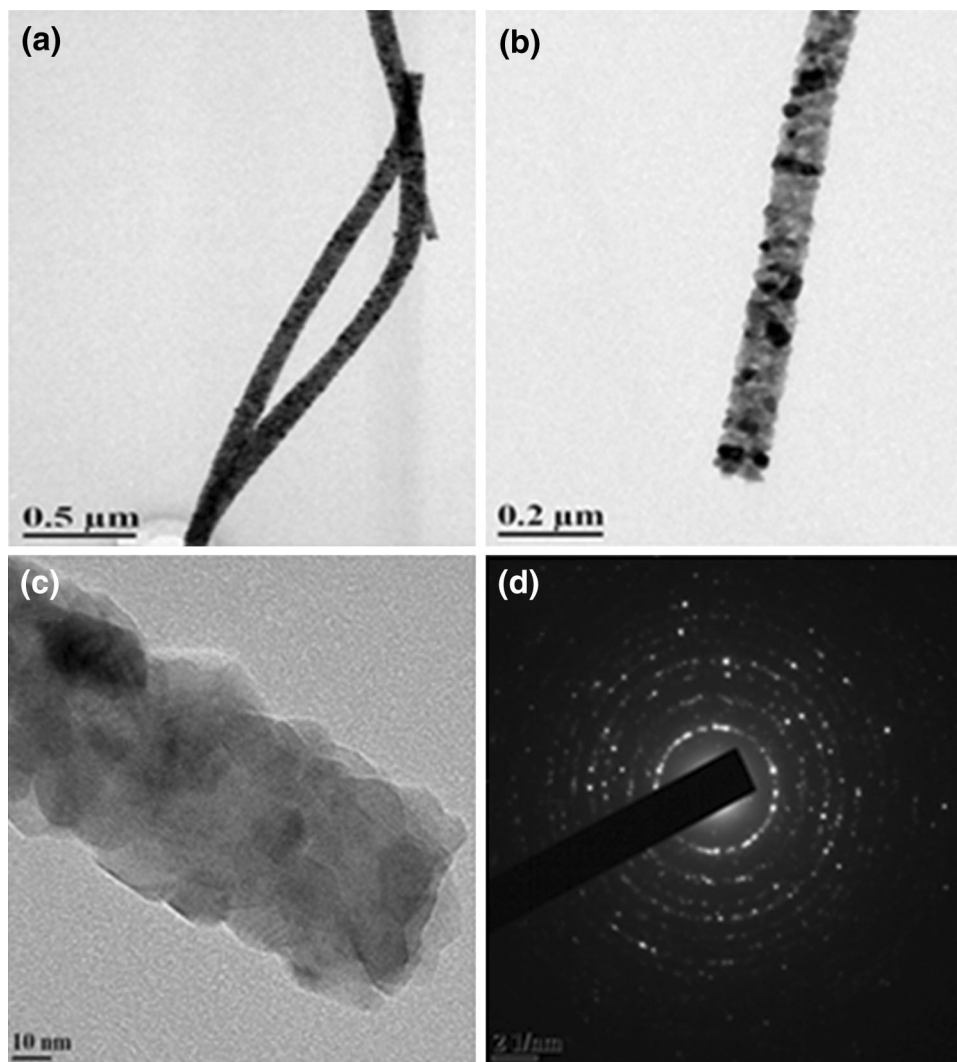


Table 1 Results of BET surface analysis of TiO₂ NFs obtained by using different wt% of PVP

Analysis	% of PVP		
	5	8	10
BET surface area (m ² /g)	29.40	26.21	20.62
Pore size (nm)	15.05	11.55	11.47
Pore volume (cm ³ /g)	0.127	0.086	0.072
Diameter (nm)	98	121	127

forward electrons transfer and suppressed the back recombination. The R_{ct2} value decreases with increase in J_{sc} value of the DSSC (Table 3). The increase in J_{sc} is due to highly porous TiO₂ NFs, which have direct pathway for electron transport due to its one-dimensional (1D) TiO₂ NFs network, resulting in faster electron transport and charge collection efficiency [20, 31–33]. It offers a low

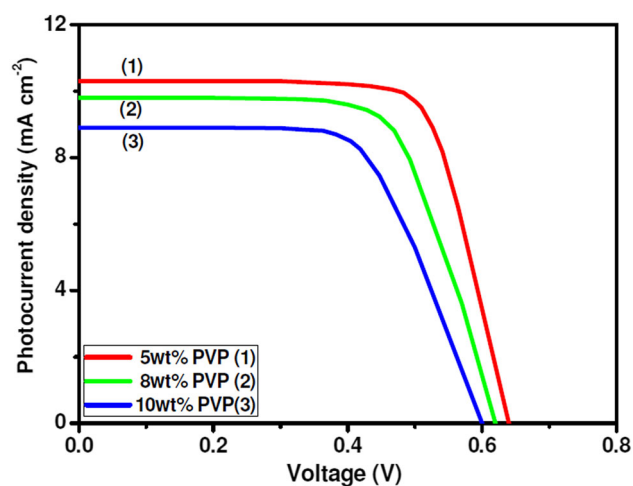
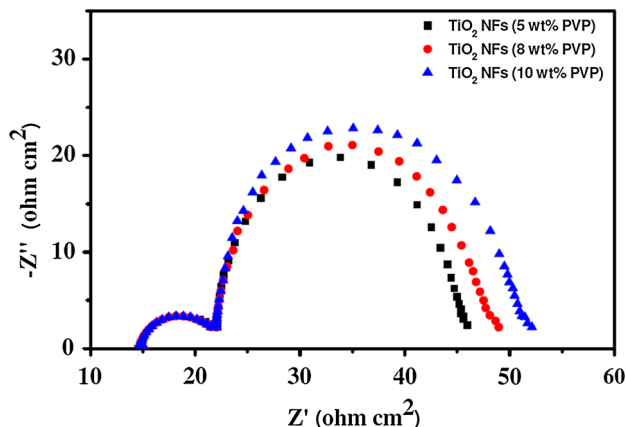


Fig. 6 Photocurrent density–voltage characteristics of TiO₂ NFs obtained by using different wt% of PVP

Table 2 Photovoltaic parameters of DSSCs assembled with TiO₂ NFs as photoanodes obtained by using different wt% of PVP

Amount of PVP used to obtain TiO ₂ NFs	J_{sc} (mA cm ⁻²)	V_{oc} (V)	FF	η (%)
5 wt%	10.3	0.64	73	4.81
8 wt%	9.8	0.62	68	4.13
10 wt%	8.9	0.60	64	3.42

**Fig. 7** Nyquist plots of DSSCs assembled with TiO₂ NFs obtained**Table 3** Electrochemical impedance parameter values of DSSCs assembled with TiO₂ NFs obtained by using different wt% of PVP as photoanode

Photoanode	R_s (Ω cm ⁻²)	R_{ct1} (Ω cm ⁻²)	R_{ct2} (Ω cm ⁻²)
TiO ₂ NFs (5 wt% PVP)	15.06	6.89	23.84
TiO ₂ NFs (8 wt% PVP)	15.11	6.97	26.89
TiO ₂ NFs (10 wt% PVP)	15.14	7.06	29.93

degree of charge recombination, thereby improving the photovoltaic efficiency of DSSC.

4 Conclusion

The porous TiO₂ NFs have successfully prepared by a simple electrospinning technique by using different wt% of PVP at the calcination temperature of 475 °C for 5 h in air. They were observed by FE-SEM and TEM analyses. It was also observed that the TiO₂ NFs obtained by using 5 wt% of PVP had larger surface to volume ratio than those obtained by using 8 and 10 wt % of PVP. Thus, a larger amount of dye adsorbed on the porous TiO₂ NFs surface increased the light-harvesting effect, thereby increasing the PCE of the DSSC. Further, it is also proven that the direct pathway for electron transport associated with one-

dimensional (1D) TiO₂ NFs network offered a low degree of charge recombination, which favors in improving the photovoltaic efficiency of the DSSC.

Acknowledgments One of the authors, Dr. AS gratefully acknowledge the UGC-DAE Consortium for Scientific Research, Indore-452 017, India (CSR-KN/CRS-47/2013-14/647), for their financial support and the CIF, Pondicherry University for extending the instrumentation facilities.

References

1. B. O'Regan, M. Grätzel, *Nature* **353**, 737 (1991)
2. M.Y. Song, D.K. Kim, K.J. Ihn, S.M. Jo, D.Y. Kim, *Nanotechnology* **15**, 1861 (2004)
3. C. Wessel, R. Ostermann, R. Dersch, B.M. Smarsly, *J. Phys. Chem. C* **115**, 362 (2011)
4. D. Hwang, S.M. Jo, D.Y. Kim, V. Armel, D.R. MacFarlane, S.-Y. Jang, A.C.S. *Appl. Mater. Interfaces* **3**, 1521 (2011)
5. S. Ramakrishnan, M. Dhakshnamoorthy, E.J. Jelmy, R. Vasanthakumari, N.K. Kothurkar, *RSC Adv.* **4**, 9743 (2014)
6. S. Valencia, X. Vargas, L. Rios, G. Restrepo, J.M. Marín, *J. Photochem. Photobiol. A Chem.* **251**, 175 (2013)
7. X.-M. Yan, J. Kang, L. Gao, L. Xiong, P. Mei, *Appl. Surf. Sci.* **265**, 778 (2013)
8. L. Zhu, K. Liu, H. Li, Y. Sun, M. Qiu, *Solid State Sci.* **20**, 8 (2013)
9. D. Zhang, T. Yoshida, K. Furuta, H. Minoura, *J. Photochem. Photobiol. A Chem.* **164**, 159 (2004)
10. D.-Y. Choi, C.-H. Hwang, J.-W. Lee, I.-H. Lee, I.-H. Oh, J.-Y. Park, *Mater. Lett.* **106**, 41 (2013)
11. W.H. Jung, N.-S. Kwak, T.S. Hwang, K.B. Yi, *Appl. Surf. Sci.* **261**, 343 (2012)
12. J.-S. Lee, Y.-I. Lee, H. Song, D.-H. Jang, Y.-H. Choa, *Curr. Appl. Phys.* **11**, S210 (2011)
13. E. Vijayakumar, A. Subramania, Z. Fei, P.J. Dyson, *RSC Adv.* **5**, 52026 (2015)
14. M.Y. Song, D.K. Kim, K.J. Ihn, S.M. Jo, D.Y. Kim, *Synth. Met.* **153**, 77 (2005)
15. S.K. Ahn, T. Ban, P. Sakthivel, J.W. Lee, Y.-S. Gal, J.-K. Lee, M.-R. Kim, S.-H. Jin, A.C.S. *Appl. Mater. Interfaces* **4**, 2096 (2012)
16. D. Li, Y. Xia, *Nano Lett.* **3**, 555 (2003)
17. Y.P. Lin, Y.Y. Chen, Y.C. Lee, Y.W. Chen-Yang, *J. Phys. Chem. C* **116**, 13003 (2012)
18. V. Thavasi, G. Singh, S. Ramakrishna, *Energy Environ. Sci.* **1**, 205 (2008)
19. H.H. Chun, W.K. Jo, *J. Ind. Eng. Chem.* **20**, 1010 (2014)
20. C. Gao, X. Li, X. Zhu, L. Chen, Z. Zhang, Y. Wang, Z. Zhang, H. Duan, E. Xie, *J. Power Sources* **264**, 15 (2014)
21. K. Mukherjee, T.-H. Teng, R. Jose, S. Ramakrishna, *Appl. Phys. Lett.* **95**, 012101 (2009)
22. S. Chuangchote, T. Sagawa, S. Yoshikawa, *Appl. Phys. Lett.* **93**, 033310 (2008)
23. W. Nuansing, S. Ninmuang, W. Jarernboon, S. Maensiri, S. Seraphin, *Mater. Sci. Eng., B* **131**, 147 (2006)
24. A.S. Nair, R. Jose, Y. Shengyuan, S. Ramakrishna, *J. Colloid Interface Sci.* **353**, 39 (2011)
25. S. Madhugiri, B. Sun, P.G. Smirniotis, J.P. Ferraris, K.J. Balkus, *Microporous Mesoporous Mater.* **69**, 77 (2004)
26. P. Pratheep, E. Vijayakumar, A. Subramania, *Appl. Phys. A* **119**, 497 (2015)
27. A.R.S. Priya, A. Subramania, Y.-S. Jung, K.-J. Kim, *Langmuir* **24**, 9816 (2008)

28. E. Vijayakumar, A. Subramania, Z. Fei, P.J. Dyson, *J. Appl. Polym. Sci.* **132**, 42032 (2015)
29. W. Chang, F. Xu, X. Mu, L. Ji, G. Ma, J. Nie, *Mater. Res. Bull.* **48**, 2661 (2013)
30. J. Watthanaarun, V. Pavarajarn, P. Supaphol, *Sci. Technol. Adv. Mater.* **6**, 240 (2005)
31. Z. Salam, E. Vijayakumar, A. Subramania, *RSC Adv.* **4**, 52871 (2014)
32. W. Wu-Qiang, L. Bing-Xin, R. Hua-Shang, X. Yang-Fan, W. Yu-Fen, S. Cheng-Yong, K. Dai-Bin, *Sci. Rep.* **3**, 1352 (2013)
33. L. Chen, X. Li, Y. Wang, C. Gao, H. Zhang, B. Zhao, F. Teng, J. Zhou, Z. Zhang, X. Pan, E. Xie, *J. Power Sources* **272**, 886 (2014)